



Novel PGK1 determines SKP2-dependent AR stability and reprograms granular cell glucose metabolism facilitating ovulation dysfunction

Xia Liu^{a,b,c,#}, Changfa Sun^{a,b,c,#}, Kexin Zou^{a,b,c}, Cheng Li^{a,b,c}, Xiaojun Chen^{a,b,c}, Hangchao Gu^{a,b,c}, Zhiyang Zhou^{a,b,c}, Zuwei Yang^{a,b,c}, Yaoyao Tu^{a,b,c}, Ningxin Qin^{a,b,c}, Yiran Zhao^{a,b,c}, Yimei Wu^{a,b,c}, Yicong Meng^{a,b,c}, Guolian Ding^{a,b,c}, Xinmei Liu^{a,b,c,*}, Jianzhong Sheng^d, Chuanjin Yu^{a,b,c,*}, Hefeng Huang^{a,b,c,*}

^a International Peace Maternity and Child Health Hospital, Shanghai Jiao Tong University School of Medicine, Shanghai, China

^b Shanghai Key Laboratory of Embryo Original Diseases, Shanghai, China

^c Institute of Embryo-Fetal Original Adult Diseases Affiliated to Shanghai Jiao Tong University School of Medicine, Shanghai, China

^d Department of Pathology and Pathophysiology, School of Medicine, Zhejiang University, Hangzhou, China

ARTICLE INFO

Article History:

Received 15 June 2020

Revised 8 September 2020

Accepted 23 September 2020

Available online xxx

Keywords:

Phosphoglycerate kinase 1
Androgen receptor
Ubiquitin ligase skp2
Glucose metabolism
PCOS

ABSTRACT

Background: Disordered folliculogenesis is a core characteristic of polycystic ovary syndrome (PCOS) and androgen receptors (ARs) are closely associated with hyperandrogenism and abnormalities in folliculogenesis in PCOS. However, whether the new AR binding partner phosphoglycerate kinase 1 (PGK1) in granulosa cells (GCs) plays a key role in the pathogenesis of PCOS remains unclear.

Methods: We identified the new AR binding partner PGK1 by co-IP (co-immunoprecipitation) in luteinized GCs, and reconfirmed by co-IP, co-localization and GST pull down assay, and checked PGK1 expression levels with qRT-PCR and western blotting. Pharmaceuticals rescue assays in mice, and metabolism assay, AR protein stability and RNA-seq of PGK1 targets in cells proved the function in PCOS.

Findings: PGK1 and AR are highly expressed in PCOS luteinized GCs and PCOS-like mouse ovarian tissues. PGK1 regulated glucose metabolism and deteriorated PCOS-like mouse metabolic disorder, and paclitaxel rescued the phenotype of PCOS-like mice and reduced ovarian PGK1 and AR protein levels. PGK1 inhibited AR ubiquitination levels and increased AR stability in an E3 ligase SKP2-dependent manner. Additionally, PGK1 promoted AR nuclear translocation, and RNA-seq data showed that critical ovulation-related genes were regulated by the PGK1-AR axis.

Interpretation: PGK1 regulated GCs metabolism and interacted with AR to regulate the expression of key ovulation genes, and also mediated cell proliferation and apoptosis, which resulted in the etiology of PCOS. This work highlights the pathogenic mechanism and represents a novel therapeutic target for PCOS.

Funding: National Key Research and Development Program of China; National Natural Science Foundation of China grant.

© 2020 The Authors. Published by Elsevier B.V. This is an open access article under the CC BY-NC-ND license (<http://creativecommons.org/licenses/by-nc-nd/4.0/>)

1. Introduction

Polycystic ovary syndrome (PCOS) is the most common endocrine and metabolic disorder in reproductive-age women, causing hirsutism, anovulatory infertility, and miscarriage [1]. PCOS is characterized by hyperandrogenism, ovulatory dysfunction, and polycystic ovaries

and is associated with other abnormalities, such as insulin resistance, metabolic syndrome, and dyslipidemia that cause women to become infertile [1,2]. However, despite the high incidence and significant health effects associated with PCOS, the pathogenic mechanism underlying PCOS development remains unclear, making mechanism-based treatments elusive.

Disordered folliculogenesis and follicle arrest are primary characteristics of PCOS. Previous studies showed that c-Fos/activator protein 1 (AP-1) and c-Jun signaling play vital roles during ovulation, primarily by promoting ovulatory gene expression [3–5]. As we know, androgens and androgen receptors (ARs) are important in PCOS because they play key roles in hyperandrogenemia prevalence and follicular development [6]. Androgens bind to the AR, which is a

* Correspondence authors: International Peace Maternity and Child Health Hospital, Shanghai Jiao Tong University School of Medicine, 910, Hengshan Road, Shanghai 200030, China

E-mail addresses: nanlilac@hotmail.com (X. Liu), Yuchuanjin1013@163.com (C. Yu), huanhgef@sytu.edu.cn (H. Huang).

These authors have equal contribution to the work.

Research in context

Evidence before this study

Polycystic ovary syndrome (PCOS) is the main cause of infertility in women. The follicles in women with PCOS generally cannot develop into a dominant follicle, resulting in ovulation dysfunction. The granulosa cell layers around these follicles show atresia, hypertrophy and degradation, suggesting metabolism dysfunction or proliferation abnormality. It is crucial that granulosa cells provide nutrients and growth regulators for oocytes during development. Therefore, their dysfunction may be one of the key factors in PCOS folliculogenesis failure.

Previous studies demonstrated that follicles in development mainly depend on the surrounding granulosa cells for energy via glycolysis. Wang et al. indicated that PCOS patients had signs of glycolysis abnormality and accompanying mitochondrial dysfunction, which influenced the switch between metabolic and glycolytic energy. However, up to now, the molecular mechanism of the key glycolysis enzyme phosphoglycerate kinase 1 (PGK1) in disordered folliculogenesis in PCOS is not clear.

Added value of this study

In the present study, we identified PGK1 as a novel binding partner of AR by mass spectroscopy in patient GCs, and showed that the abundance of PGK1 was increased in PCOS luteinized GCs and PCOS-like mouse ovarian tissues by qRT-PCR and western blotting. PGK1 regulated glucose metabolism and deteriorated the PCOS-like mouse metabolic disorder. Meanwhile, highly abundant PGK1 inhibited AR ubiquitination levels and increased AR stability in an E3 ligase SKP2-dependent manner. In addition, RNA-seq data showed that critical ovulation-related genes were regulated by the PGK1-AR axis. Previous study demonstrated impaired development of follicles and low oocyte competence in PCOS. Thus, our data indicate that the reason for folliculogenesis failure might be excessive expression of critical ovulation-related genes and glucose dysfunction.

Implications of all the available evidence

In this study, PGK1 was highly expressed in PCOS luteinized GCs and PCOS-like mouse ovarian tissues, and the high expression levels were related to hyperandrogenemia. The PGK1 in GCs regulated metabolism interacted with AR to mediate the expression of key ovulation genes and regulated cell proliferation and apoptosis, resulting in the etiology of PCOS. This provided us a new mode of action for abnormal glycolysis in PCOS, and also a potential treatment target for clinical PCOS.

(HIF-1) transcribes and activates PGK1 in breast cancer, and PGK1 might be as the primary target molecule in colorectal cancer cells during immunotherapy [11,12]. In addition, PGK1 acts as a protein kinase that regulates mitochondrial function and autophagy induced by cell stress [9]. The key functions of PGK1 in the comprehensive regulation of glycolysis, mitochondrial metabolism, and autophagy serve to promote tumor cell proliferation and maintain of cell homeostasis [13–15]. Of note, PGK1 plays an important role in metabolic reprogramming, resulting in the conversion of glucose into lactate. PCOS is associated with many risk factors in adults, including insulin resistance and gestational diabetes, and is closely associated with reproductive failure and dysfunctional metabolism [16,17]. It remains unclear whether PGK1 bind with AR and regulates glucose metabolism in GCs, leading to insulin resistance and other PCOS-associated metabolic disorders, and whether it regulates c-Fos or c-Jun signaling during ovulation. The present study identified new functions of the PGK1-AR axis in the reproductive system, which may represent a new therapeutic target for PCOS.

2. Materials and methods

2.1. Ethics statement

This study was approved by the Ethics Committee of the International Peace Maternity and Child Health Hospital, School of Medicine, Shanghai Jiao Tong University, Shanghai, China. Ovarian GCs were collected from patients who underwent in vitro fertilization (IVF) at the Center for Reproductive Medicine of International Peace Maternity and Child Health Hospital. Signed informed consent was received from all subjects (NO. GKLW 2015–42). PCOS patients were identified by the Rotterdam diagnostic criteria and the patient luteinized GCs were retrieved from the follicular fluid. The follicular fluid was collected and centrifuged at 20 min 2000 rpm and the pellets were re-suspended in phosphate-buffered saline containing 0.1% hyaluronidase (Sigma-Aldrich, St. Louis, MO, USA) at 37 °C for 20 min. Then, granulosa cells were purified by Ficoll-Paque separation (GE Healthcare Bio-Science, Uppsala, Sweden) and used for the next study. The procedures for animal experiments were performed following the Guide for the Care and Use of Laboratory Animals at Shanghai Model Organisms (Shanghai, China) and the approval ID for the animal experiment was 2018–0005.

2.2. Cell culture

The human cell line HEK293T and the human ovarian granulosa-like tumor cell line KGN were preserved in the central laboratory of the International Peace Maternity and Child Health Hospital. HEK293T cells were cultured in Dulbecco's modified Eagle medium (DMEM, Gibco, BRL, Grand Island, NY, USA) with 10% foetal bovine serum (FBS, Gibco) and 1% penicillin-streptomycin. KGN cells were cultured in DMEM/F12 (Gibco) with 10% FBS and 1% penicillin-streptomycin (Gibco). The cell line information and other materials in this study are described in [Supplementary Table 1](#).

2.3. Plasmids and lentivirus

The polymerase chain reaction (PCR) products were generated by a PCR instrument (Applied Biosystems, Foster City, CA, USA). It was programmed for 35 cycles, and each cycle consisted of pre-denaturation at 95 °C for 120 s followed by denaturation at 95 °C for 25 s, annealing at 57 °C for 29 s, and extension at 72 °C for 60 s. PCR-amplified full-length sequences of human *PGK1* and *AR* were cloned into pFLAG-CMV-2 and pcDNA-HA. The structural domains of PGK1 were generated from full-length PGK1 and cloned into pEGFP-C1. The lentiviral vectors shCtrl and shPGK1 were purchased commercially (Genepharma, Shanghai, China). Plasmids were transfected into

transcription factor belonging to a superfamily of steroid hormone receptors and primarily functions by modulating genomic activity as a nuclear receptor [7]. In the ovary, the AR is primarily expressed by granulosa cells (GCs), during most stages of follicular development. In our previous study, phosphoglycerate kinase 1 (PGK1) was identified as a new binding partner with the AR in GCs [8], but whether it cooperated with AR in folliculogenesis or PCOS was really unknown.

PGK is one of two enzymes that produce ATP during glycolysis, regulating energy homeostasis. It catalyses the conversion of 1,3-bisphosphoglycerate into 3-phosphoglycerate, which generates ATP during glycolysis [9,10]. In humans, two PGK isoenzymes, PGK1 and PGK2, have been identified. Researchers have examined the roles played by PGK1 in many diseases and the associated underlying molecular mechanisms. For example, hypoxia-inducible factor-1

HEK293T cells in 6-well plates. Cells were seeded 24 h in advance, and the cell density was approximately 80% at the time of transfection. Transfection was performed using 2 μ g of plasmid and 5 μ L Lipo2000 (Invitrogen, Carlsbad, CA, USA) according to the manufacturer's protocol. Cells were collected 36 h after transfection. KGN cells were seeded into 6-well plates 24 h before transfection with the lentivirus and the medium was replaced with fresh DMEM/F12 before transfection. The quantitative real-time PCR (qRT-PCR) and western blotting experiments were performed to verify the mRNA and protein levels, respectively.

2.4. Western blotting

Cells were lysed using lysis buffer (P0013, Beyotime, Nanjing, Jiangsu, China), containing protease inhibitor cocktail (YEASEN, Shanghai, China). Protein concentrations were determined by bicinchoninic acid assay (Thermo Fisher Scientific, Rochester, NY, USA). A total of 20 μ g of each protein extract was separated by sodium dodecyl sulfate (SDS)-polyacrylamide gel electrophoresis (PAGE) and blotted onto a polyvinylidene difluoride (PVDF) membrane. The PVDF membrane was blocked with 5% milk for 1 hr. Then, the membrane was incubated with the relevant antibody at 4 °C overnight. After washing three times with Tris-buffered saline containing Tween20 (TBST), the membrane was incubated with horseradish peroxidase (HRP)-conjugated secondary antibody. Relative protein levels were quantified by Image J.

2.5. RNA-seq and qRT-PCR

The KGN cells treated with shRNA PGK1 in advance were seeded in 9 cm plates and serum starved for 12 hrs, before stimulation by DHT (final concentration 10–7 mol•L⁻¹) for 24 hrs. The cells from each group were collected and sent to Novel Bioinformatics Ltd., Co. (Shanghai, China) for RNA-seq and bioinformatics analysis. The RNA-seq data were deposited in the NCBI (National Center for Biotechnology Information) GEO depository and assigned accession numbers is GSE146856. Total RNA from cultured cells, human GCs, and mouse ovarian tissues were isolated with RNAisoreagent (9109, Takara, Shiga, Japan), according to the manufacturer's instructions. According to the protocol, a total of 1 μ g of RNA was synthesized into cDNA using the RT Reagent Kit and gDNA Eraser (RR047A, Takara, Shiga, Japan). The qRT-PCR was performed on the QuantStudio 7 Flex system (Life Technologies, Carlsbad, CA, USA). All samples were run in triplicate. To quantify the relative expression of mRNA, data were normalised to the expression level of glyceraldehyde 3-phosphate dehydrogenase (GAPDH). The primers and si-RNAs in the study are described in [Supplementary Table 2](#).

2.6. Immunofluorescence staining

Cultured cells were washed with phosphate-buffered saline (PBS), then fixed with 4% paraformaldehyde for 15 min. After washing with PBS, cells were permeabilised with 1% Triton-100 for 15 min. After blocking in 3% bovine serum albumin for 1 h, cells were incubated with primary antibody overnight at 4 °C. After washing with PBS, cells were incubated with Alexa Fluor 488- or 594-conjugated secondary antibodies (Invitrogen) for 1 h and then stained with the nuclear stain 4',6-diamidino-2-phenylindole (DAPI), at room temperature. Immunofluorescence was detected using a confocal microscope.

2.7. Immunoprecipitation assays

Cells were lysed with IP lysis buffer (P0013, Beyotime). The whole-cell lysates were incubated with antibodies overnight at 4 °C and then precipitated with the antibody-protein complex, using

Protein A/G beads (Thermo Fisher Scientific). The immunoprecipitates were washed five times and then subjected to western blotting analysis.

2.8. Cell counting kit-8 (cck-8) assay, colony formation assay, and terminal deoxynucleotidyltransferase dUTP nick labeling (TUNEL) assay

For the CCK-8 assay, 2000 cells were seeded in 96-well plates for 24 hrs. After treatment with dimethyl sulfoxide (DMSO), DHT, and relative cell growth was measured using a Cell Counting Kit-8 (YEASEN), according to the manufacturer's protocol. For colony formation assays, 2000 cells were seeded in 6-well plates and cultured overnight. Cells were cultured in the presence or absence of DHT in complete media for 14 days. The medium was discarded and the cells were washed once with PBS. Cells were then fixed in methanol, at room temperature for 10 min. The methanol was discarded, and cells were washed with PBS three times. Giemsa stain was added to each well for 30 min and discarded, and cells were washed with PBS. The images were taken by a digital camera and the colony numbers were analyzed by the Image J software. For apoptosis assays, cells were seeded in 15-mm cell culture dishes and cultured in complete medium for 1 day. Cells were incubated at 37 °C for 6 h, in the presence or absence of DHT. A TUNEL kit (C1089, Beyotime), was used according to the manufacturer's protocol. Images were acquired by confocal microscope.

2.9. The glutathione-S-transferase (GST) pull-down assay and kinase assay in vitro

The expression of GST, GST-PGK1, and His-AR proteins was induced in *E. coli* BL2, grown in LB-ampicillin and harboring the plasmids pGEX-4T1, pGEX4T-PGK1, and pET-28a-AR, respectively, using isopropyl β -D-1-thiogalactopyranoside when cells reached an optical density of approximately 0.6. Proteins were expressed at 28 °C overnight. Then, the bacterial liquid was collected, the supernatant was removed by centrifugation, and an appropriate amount of PBS was added to perform ultrasonic fracture on ice. Then the mixture was centrifuged at 4 °C, at 3000 \times g for 20 min. The supernatant was collected and the proteins were purified according to the manufacturer's protocol. Purified GST-PGK1 fusion protein or GST control was combined with His-AR fusion protein and GST-agarose overnight at 4 °C. The protein mixtures were washed four times, as previously described [18]. The protein samples were separated by 10% SDS/PAGE, followed by western blotting. For the kinase assay *in vitro*, the recombinant PGK1 and AR proteins were incubated in the kinase buffer (25 mM Tris-HCl at pH 7.5, 10 mM MgCl₂, 2 mM Dithiothreitol, 5 mM β -glycerophosphate, 0.1 mM Na₃VO₄, and 10 mM ATP) (Sigma-Aldrich). The reactions were incubated at 37 °C for 25 min, followed by western blotting.

2.10. PCOS-like mouse model

Female C57BL/6 J mice were purchased commercially (Shanghai Model Organisms, Shanghai, China). Mice were obtained at the age of 3 weeks and allowed to habituate for 1 week. The PCOS-like mouse model was generated by treating the mice daily with dehydroepiandrosterone (DHEA; 0.6 g/kg body weight) via subcutaneous injection for 20 days [19]. The PCOS-like mice in the paclitaxel (PTX) treatment group were gavaged with PTX (0.2 mg/mL) at 7 weeks-age for 3 weeks. Mouse body weights were measured weekly. The vaginal cells of the indicated mice were collected daily with normal saline lavage and visualized under light microscopy for 16 consecutive days. The standard for the oestrus cycle was identified in the following way: mainly leukocytes in the dioestrus stage, mainly nucleated cells in the pro-oestrus stage, mainly cornified epithelial cells in the oestrus stage, and a mixture of both leukocytes and cornified cells in the

metoestrus stage. To determine the ovarian morphology, ovaries were fixed in 4% paraformaldehyde, dehydrated in an ethanol gradient, and finally embedded in paraffin. Ovary tissues were sectioned to approximately 8 μm thick in succession, and the sections were stained with haematoxylin and eosin (H&E). Finally, histomorphological observation was performed with a microscope (DM2500, Leica, Germany). The cystic follicles and corpora lutea were counted, and the phenotype and the counted number were confirmed by a pathologist. The protein expression levels in the ovaries were measured by immunohistochemistry (IHC) following a series of procedures: antigen retrieval, addition of primary and secondary antibody, and finally adding a detection reagent to recognize and localize the primary antibody referenced as Magaki et al. [20].

2.11. Glucose tolerance test (GTT) and insulin tolerance test (ITT)

Mice were fasted for 12 hrs before the GTT and four hours before the ITT. The glucose concentration was checked by tail vein blood sampling using the Accu-Chek Performa blood glucose meter (Roche, Los Gatos, CA, USA). After testing the fasting glucose concentrations, the mice were intraperitoneally injected with glucose (G6152, Sigma-Aldrich) ($2 \text{ mg} \cdot \text{g}^{-1} \text{ BW}$) for the GTT, or insulin ($1000^{-1} \text{ IU} \cdot \text{g}^{-1} \text{ BW}$) for the ITT. The tail sample blood glucose levels were measured at time points 15, 30, 60, and 120 min.

2.12. Metabolism detection in cells and mice

The KGN cells were seeded in 6-well plates and manipulated with the relevant treatment, then the culture medium supernatant was collected and kits were used to detect the production of glucose (GAGO20, Sigma-Aldrich), and lactate (K607, BioVision, Milpitas, CA, USA) production according to the protocols. The cells were seeded on the plates, and the extracellular acidification rate (ECAR) and oxygen consumption rate (OCR) were measured with the Seahorse XFe96 Analyzer (Agilent Technologies, Santa Clara, CA, USA), with a method slightly modified from Chakraborty et al. [21]. The metabolic and physical parameters of the control, PCOS-like model, and PTX treatment mice were analysed by the Comprehensive Lab Animal Monitoring System (Columbus Instruments, Columbus, OH, USA). The animals were maintained under a constant temperature, (22°C), with a 12-h light/dark cycle, with free access to water and food. After proper adaptation to the system, the food intake, CO_2 and O_2 vol, respiratory exchange rate (RER), and energy expenditure of each mouse were measured for 24 h.

2.13. Statistical analysis

All calculations were performed using Excel and GraphPad Prism software (GraphPad, La Jolla, CA, USA). Data are expressed as the mean \pm SE. The statistical analysis was performed using the unpaired two-tailed Student's *t*-test. Statistical differences were considered significant at $p < 0.05$. The clinical data were analysed with SPSS v.26.0 (Endicott, New York, NY). Normally distributed continuous data were expressed as the mean \pm SE and differences between groups were compared by Student's *t*-test. Skewed variables were expressed as the median (95% confidence intervals) and analysed by Mann-Whitney U test between groups. Significance is denoted as follows: * $p < 0.05$, ** $p < 0.01$, and *** $p < 0.001$.

2.14. Role of funding source

This study was supported by the National Key Research and Development Program of China (2018YFC1003201, 2017YFC1001300), International Cooperation Project of China and Canada NSFC (81661128010), the National Natural Science Foundation of China (81671412, 81771593), Chinese Academy of Medical

Sciences Research Unit (No. 2019RU056), CAMS Innovation Fund for Medical Sciences (CIFMS) (2019-I2M-5-064), The Interdisciplinary Key Program of Shanghai Jiao Tong University (YG2014ZD08), Shen Kang Three Year Action plan (16CR3003A), the postdoctoral grant (2018M630454), Shanghai Municipal Key Clinical Specialty, Shanghai, China. The funding sources had no role in the study design, interpretation of data and collection analysis, writing of the report, and the decision to submit the paper for publication.

3. Results

3.1. PGK1 and ar are highly expressed in the GCs of patients with PCOS

Our previous study used AR as the bait to identify PGK1 as a new binding partner [8]. AR co-immunoprecipitation (co-IP) proteins from human GCs were analysed by mass spectrometry, which identified PGK1 binding to AR (Figs. 1a and 1b). Importantly, the mRNA expression levels of *PGK1* were higher in PCOS GCs than in non-PCOS GCs (Fig. 1c). It was also found that *PGK1* expression levels were related with clinical features in PCOS patients (Table 1). In addition, *PGK1* mRNA expression levels were positively correlated with the serum levels of testosterone (TT) and the ratio of serum LH (luteinizing hormone) to FSH (follicle stimulating hormone) among patients (Figs. 1d and e). Furthermore, western blotting analysis showed that both PGK1 and AR protein expression levels were high in PCOS GCs (Fig. 1f and 1g). These results demonstrate that PGK1 may be involved in PCOS, likely through the AR pathway.

3.2. PGK1 is associated with ovulatory obstacles, and the phenotype can be rescued by PTX

A previous study demonstrated that PGK1 plays vital roles in both physiological and pathological processes, due to its effects on cell proliferation and apoptosis [9,10]. PTX is one of the most effective chemotherapeutic drugs used for the treatment of ovarian cancers and acts by arresting the cell cycle, causing apoptosis [22]. Here, we used PTX as a candidate drug to counteract the effects of PGK1 during PCOS treatment. A PCOS-like mouse model was successfully established, showing abnormal oestrus cycles and increased cystic follicles, and these abnormal PCOS-like symptoms were attenuated by PTX treatment (Figs. 2a and 2b). The number of mouse embryos produced by DHEA-treated PCOS-like mice decreased significantly compared to that of the control, whereas the number of embryos increased after PTX treatment (Fig. 2c). Western blotting and immunohistochemical analyses showed that the PGK1 and AR protein expression levels in PCOS-like mice were high in ovarian tissue but returned to normal levels after PTX treatment (Figs. 2d and 2e). This suggests that PTX treatment reduced PGK1 protein expression and provides further evidence that PGK1 is associated with ovulatory obstacles via AR signaling. Importantly, we also found that the ovulation-related phosphorylation levels of the c-Fos and c-Jun signaling pathways increased in the PCOS-like group and decreased in the PTX group, to levels similar to those observed in the control group (Fig. 2f). In addition, the TUNEL assay showed that the ovarian GCs in PCOS-like mice did not undergo apoptosis but that PTX was able to induce apoptosis in these cells (Fig. 2g). The Ki-67 staining data demonstrated the increased proliferation of ovarian GCs in PCOS-like mice that was reduced by PTX treatment (Fig. 2h). The effects of PTX on GC cells were likely associated with the rescue of the critical ovulation-associated c-Fos and c-Jun phosphorylation levels, which may promote GC apoptosis, resulting in successful ovulation.

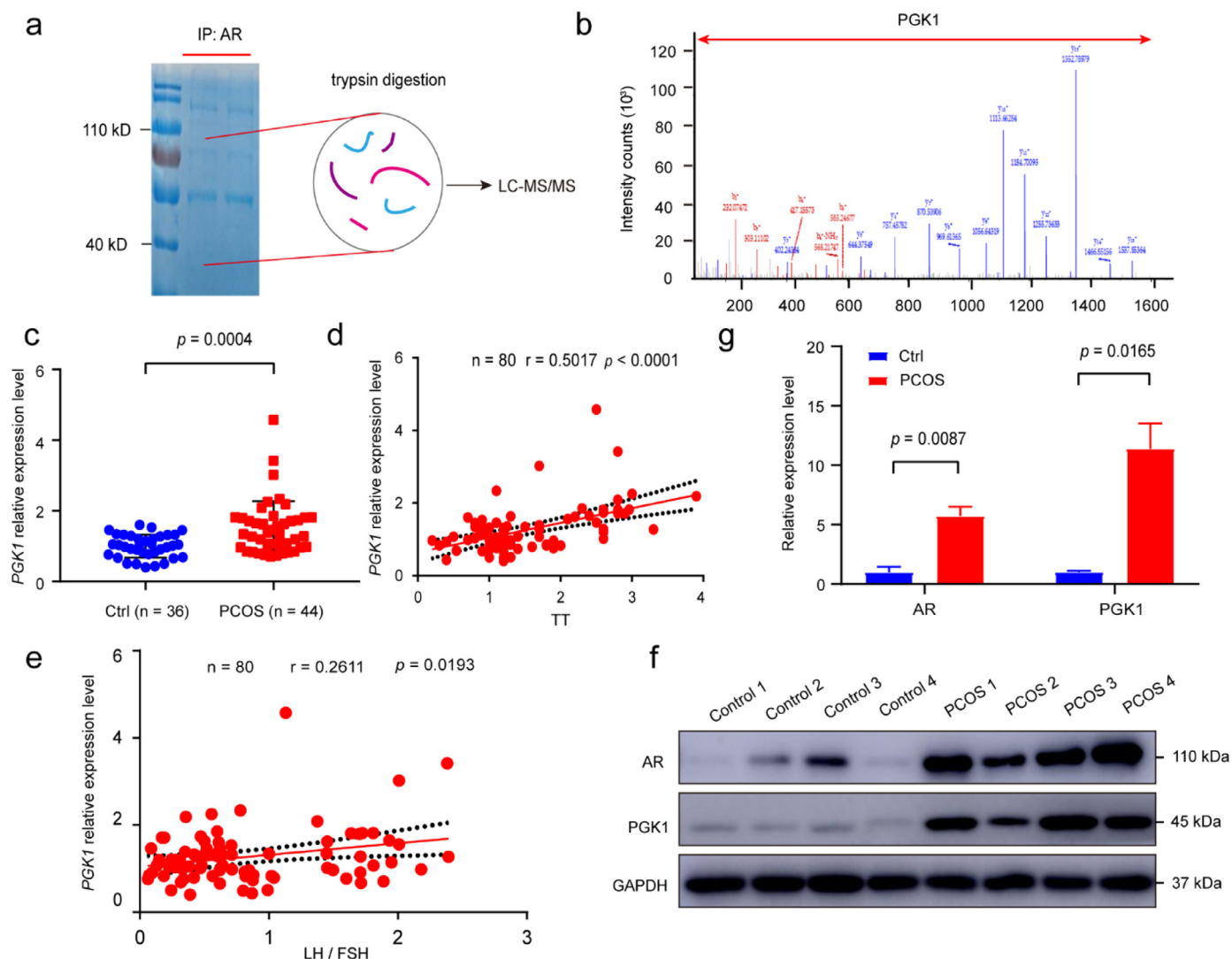


Fig. 1. PGK1 is a new binding partner for AR, and PGK1 and AR protein levels are highly expressed in human PCOS luteinized granulosa cells (GCs) were used for a co-immunoprecipitation (co-IP) assay, with an AR antibody, and the proteins were separated by 10% SDS/PAGE, followed by Coomassie staining. Next, the gel was cut into strips containing the proteins of interest, treated with trypsin digestion, and analysed by LC-MS/MS. (b) Mass spectroscopy identified PGK1 as a new protein partner of the AR protein. (c) The relative expression level of *PGK1* mRNA in human luteinized GCs from the Control ($n = 36$) and PCOS groups ($n = 44$). Data are expressed as the mean \pm SE. The p values were calculated by an unpaired two-tailed Student's t -test compared with controls. (d) Correlation analysis between the relative expression levels of *PGK1* mRNA and serum testosterone (TT) levels among patients ($r = 0.5017$, $p < 0.0001$, $n = 80$). (e) Correlation analysis between the relative expression levels of *PGK1* mRNA and the ratio of serum LH (luteinizing hormone) to FSH (follicle stimulating hormone) among patients ($r = 0.2611$, $p = 0.0193$, $n = 80$). (f-g) PGK1 and AR protein were detected by western blotting analysis in human luteinized GCs from patients in the Control and PCOS ($n = 4$ per group). The protein expression levels of PGK1 and AR were statistically analysed. Data are expressed as the mean \pm SE. The p values were calculated by an unpaired two-tailed Student's t -test compared with controls.

3.3. PGK1 regulates cell glucose metabolism and aggravates metabolic disorders in PCOS-like mice

PGK1 plays a vital role in glycolysis, converting glucose into lactic acid. We examined whether the PGK1 regulation of glucose metabolism played a role in PCOS. Thus, we first used KGN cells to measure glucose and lactate production. The glucose levels in shPGK1 (PGK1 knockdown) cells increased, whereas the glucose levels in overexpression (OE)-PGK1 cells decreased, compared with the levels in control (Ctrl) cells. In contrast, lactate levels were reduced in shPGK1 cells and increased in OE-PGK1 cells relative to Ctrl cell levels (Figs. 3a and 3b). In addition, the extracellular acidification rate (ECAR) was notably downregulated and the OCR was notably upregulated in shPGK1 cells (Figs. 3c and 3d) compared to Ctrl cells. Meanwhile, the gene set enrichment analysis (GSEA) and the glucose metabolism genes were significantly regulated by PGK1 in the shPGK1 cells compared to control RNA-seq data, indicating that PGK1 plays a key role in the regulation of glucose metabolism in GCs

(Supplementary Figure 1 and Supplementary Figure 2). Next, we assessed the whole-body glucose homeostasis of PGK1 in PCOS-like mice. The weight curves for the mice showed that the body weights for the PCOS-like group were higher than those for the Ctrl group. The PCOS+PTX group had body weights similar to those of the PCOS group, and the area under the curve (AUC) analysis showed similar results (Figs. 3e and 3f). The homeostasis model assessment-insulin resistance (HOMA-IR) values in the PCOS+PTX group decreased compared with those in the PCOS-like group (Fig. 3g). Glucose and insulin resistance were increased in PCOS-like mice compared to in Ctrl mice, and PTX was able to reduce the glucose and insulin resistance of PCOS-like mice to Ctrl levels (Figs. 3h–3m). Insulin secretion defects contribute to glucose intolerance, and our results showed that insulin secretion in PCOS-like mice was reduced compared with that of both the Ctrl and PCOS+PTX groups, but not significantly (Figs. 3n and 3o), indicating that neither the PCOS-like model nor PTX treatment influenced insulin secretion for the regulation of glucose levels. Importantly, we also evaluated the metabolic

Table 1
Characteristics of the patients in the study.

	Ctrl(n = 36)	PCOS Total PCOS(n = 44)	PCOS-NHT(n = 28)	PCOS-HT(n = 16)
Age, year [§]	31.66±4.44	31.66±4.44	31.50±6.50	30.00±5.50
Height, cm [§]	161.23±5.45	161.23±5.45	160.00±6.25	160.00±4.50
Body weight, kg [§]	60.60±7.97	60.60±7.97	60.96±1.41	59.97±2.24
BMI, kg/m ² [§]	23.29±2.69	23.29±2.69* [#]	23.54±0.42	22.85±0.86
Cycle length, days [‡]	30.00(28.00–30.00)	41.50(31.25–90.00) ^{***,§}	45.00(35.00–90.00)	37.50(28.00–82.50)
Duration of infertility, Year [‡]	2.50(1.00–4.75)	3.00(2.00–5.00)	4.00(2.00–5.75)	3.00(1.25–4.00)
FSH, IU/L [‡]	8.35(5.98–10.00)	6.80(5.60–10.20)	6.25(5.25–8.54)	9.05(6.08–13.65)
LH, IU/L [‡]	4.50(3.60–5.97)	5.20(3.35–9.48)	5.50(3.13–9.18)	4.60(3.63–12.13)
PRL [‡]	11.85(9.35–18.93)	12.95(8.25–16.03)	13.15(8.25–15.00)	12.35(8.00–17.48)
Day 3 serum TT, nmol/L [‡]	1.00(0.80–1.20)	2.05(1.43–2.60) ^{***,§}	1.70(1.26–1.98)	2.80(2.60–2.95) ^{i,***,§}
Day 3 serum E2, pmol/L [‡]	136.50(85.50–204.50)	143.00(96.50–223.75)	129.50(82.75–204.25)	194.50(104.25–269.75)
Day 3 serum Prog, nM [‡]	2.00(1.00–4.13)	2.00(1.00–2.80)	2.00(1.00–3.10)	2.00(1.05–2.75)
LH on HCG day, IU/L [‡]	2.40(1.35–3.10)	2.65(1.40–4.20)	2.60(1.25–3.63)	3.20(1.73–8.03)
E ₂ on HCG day, IU/L [‡]	10,627.00(5178.25–16,666.75)	16,405.00(9427.00–17,827.00) ^{*,§}	14,774.50(11,495.00–17,827.00)	17,827.00(7923.00–18,121.00)
Prog on HCG day, nM [‡]	2.70(1.95–4.95)	3.40(1.60–4.98)	3.30(1.60–5.05)	3.75(1.68–4.98)

* indicates PCOS patients versus control (Ctrl).

[†] * indicates PCOS-HT patients versus PCOS-NHT. HT means high testosterone, NHT means non-high testosterone.

* $P < 0.05$.

*** $P < 0.001$.

[§] Mean±SE.

[#] unpaired *t*-tests.

※ Median (range).

[§] Mann-Whitney *U* test.

characteristics of the three groups of mice. There were no significant differences in food intake, O₂ vol, or physical activity along the X and Z axis among the groups (Figs. 3p–3s and Supplementary Figure 3), but the RER in PCOS-like mice was notably higher than that in Ctrl mice, which could be corrected by PTX during both the light and dark periods (Figs. 3t and 3u). Together, these results suggest that PGK1 may regulate glucose metabolism dysfunction in GCs, resulting in ovulation disorder, and that PTX was able to rescue PCOS-like metabolic disorders, likely by acting on PGK1, ameliorating glucose metabolism.

3.4. PGK1 physically interacts with the AR

In both clinical human GC samples and the PCOS-like mouse model, PGK1 and AR protein expression levels were high. However, whether they interacted with each other remained unknown. To confirm whether PGK1 binds with AR, co-immunoprecipitation (co-IP) assays were performed in HEK293T cells transfected with Flag-PGK1 and HA-AR. The results showed that PGK1 was able to bind to the AR in HEK293T cells (Figs. 4a and 4b). To further determine whether PGK1 and AR interact, the endogenous proteins were examined in a co-IP assay performed with the KGN cell line, demonstrating that PGK1 interacted with the AR, whereas the IgG control showed no visible bands (Figs. 4c and 4d). In addition, a GST pull-down assay demonstrated that PGK1 interacted directly with the AR in vitro (Fig. 4e). Furthermore, an immunofluorescence assay showed that PGK1 and AR were both primarily distributed in the nucleus (Figs. 4f and 4g). As described in a previous study [23], we also generated PGK1 structural domains fused to a green fluorescent protein (GFP)-tag (GFP-catalytic domain 1 [CD1], GFP-nucleotide-binding domain [NBD], GFP-CD2). The data illustrated that the nucleotide-binding domain (NBD) of PGK1 was the primary interaction site for AR (Fig. 4h).

3.5. PGK1 promotes AR translocation into the nucleus, and depends on ubiquitin ligase SKP2 to increase AR stability

To study the function of PGK1, we screened and obtained the best shRNA target (shRNA #3) against PGK1 (Fig. 5a). Western blotting analysis showed that total AR protein levels decreased when the KGN cell line was treated with shPGK1, which was dependent on

dihydrotestosterone (DHT) (Fig. 5b). To determine whether PGK1 could regulate the nuclear translocation of AR, we used a nucleoplasm and cytoplasm separation kit and immunofluorescence to analyze a KGN cell line treated with shPGK1 and background DHT. The results showed reduced levels of nuclear AR in KGN cells treated with shPGK1. This response was dependent on DHT (Figs. 5c and 5d), indicating that PGK1 promoted AR translocation into the nucleus.

To further investigate the relationship between PGK1 and AR, empty Flag vector or Flag-PGK1 was co-transfected with HA-AR into HEK293T cells, and PGK1 overexpression was found to increase AR protein expression levels (Fig. 5e). The expression level of AR in shPGK1-treated KGN cells was significantly lower than that in shCtrl-treated cells (Fig. 5f). Based on these results, we suspected that PGK1 might increase AR stability. To further determine whether PGK1 affected the stability of AR, KGN cells were transfected with shPGK1 and then treated with cycloheximide (CHX), an inhibitor of protein biosynthesis and MG132 (a proteasome inhibitor), for the indicated times. The results showed that AR protein levels decreased after CHX treatment in shPGK1-treated cells compared to in shCtrl-treated cells (Fig. 5g), demonstrating that PGK1 promotes AR protein stability. The ubiquitin/proteasome-mediated pathway regulates protein degradation in eukaryotic cells [24]. From our RNA-seq data, GSEA analysis showed that the ubiquitin-mediated proteolysis pathway was upregulated in shPGK1-treated cells (Fig. 5h). In addition, we detected the ubiquitination levels for AR and found that levels decreased in the presence of PGK1 compared with control levels (Fig. 5i), which further indicates that PGK1 promoted AR protein stability by regulating AR ubiquitination levels.

The heatmap shows that the core enrichment genes involved in protein ubiquitination were upregulated and one of the most significantly upregulated genes encoded E3 ubiquitin ligase S-phase kinase-associated protein 2 (SKP2) (Fig. 5j). Next, we determined whether the observed PGK1-mediated increase in AR protein stability was dependent on the E3 ubiquitin ligase SKP2. The AR protein level increased notably when cells were treated with si-SKP2 compared with the control level, while the AR protein levels did not increase when we introduced PGK1 into the cells once again (Fig. 5k), which indicates that the PGK1-mediated increase in AR protein stability was dependent on the ligase SKP2.

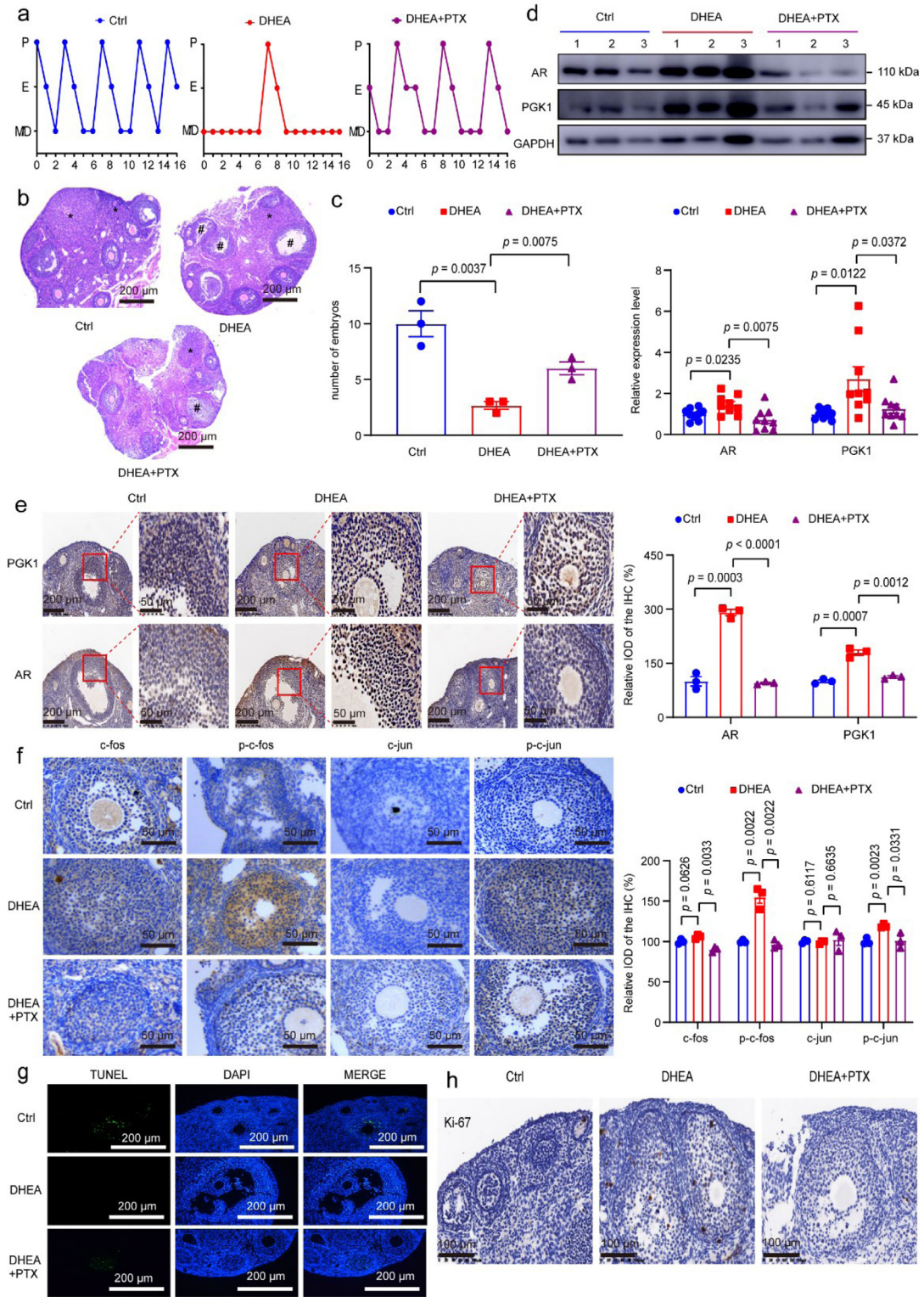


Fig. 2. PGK1 is upregulated in PCOS-like model mice and returns to normal levels after PTX treatment. (a) Continuous monitoring of the oestrus stage in the mice in three groups (Ctrl, DHEA, and DHEA+PTX). (b) Representative images of H&E-stained mouse ovaries for the indicated groups. * shows corpus luteum and # shows cystic follicles. Scale bar: 200 μ m. (c) The number of embryos was analysed, and the data are expressed as the mean \pm SE ($n = 5$ per group). (d) PGK1 and AR were detected by western blotting analysis in mouse ovaries from the indicated groups ($n = 3$ per group). The protein expression levels of PGK1 and AR were analysed, and the data are expressed as the mean \pm SE. (e) Representative images of immunohistochemical staining, using PGK1- and AR-specific antibodies, of mouse ovaries from the indicated groups ($n = 5$ per group). Data are expressed as the mean \pm SE. Scale bars in the original and enlarged images are 200 μ m and 50 μ m, respectively. (f) Representative images of immunohistochemical staining, using the indicated specific antibodies for c-Fos, p-c-Fos, c-Jun and p-c-Jun, of mouse ovaries from the indicated groups ($n = 5$ per group). Data are expressed as the mean \pm SE. Scale bar: 50 μ m. (g) Representative images of TUNEL assay results in mouse ovaries from the indicated groups ($n = 3$ per group). Scale bar: 200 μ m. (h) Representative images of immunohistochemical staining, using Ki-67-specific antibodies, of mouse ovaries from the indicated groups ($n = 3$ per group). Scale bar: 100 μ m. The statistical data were analysed by an unpaired two-tailed Student's *t*-test compared with controls.

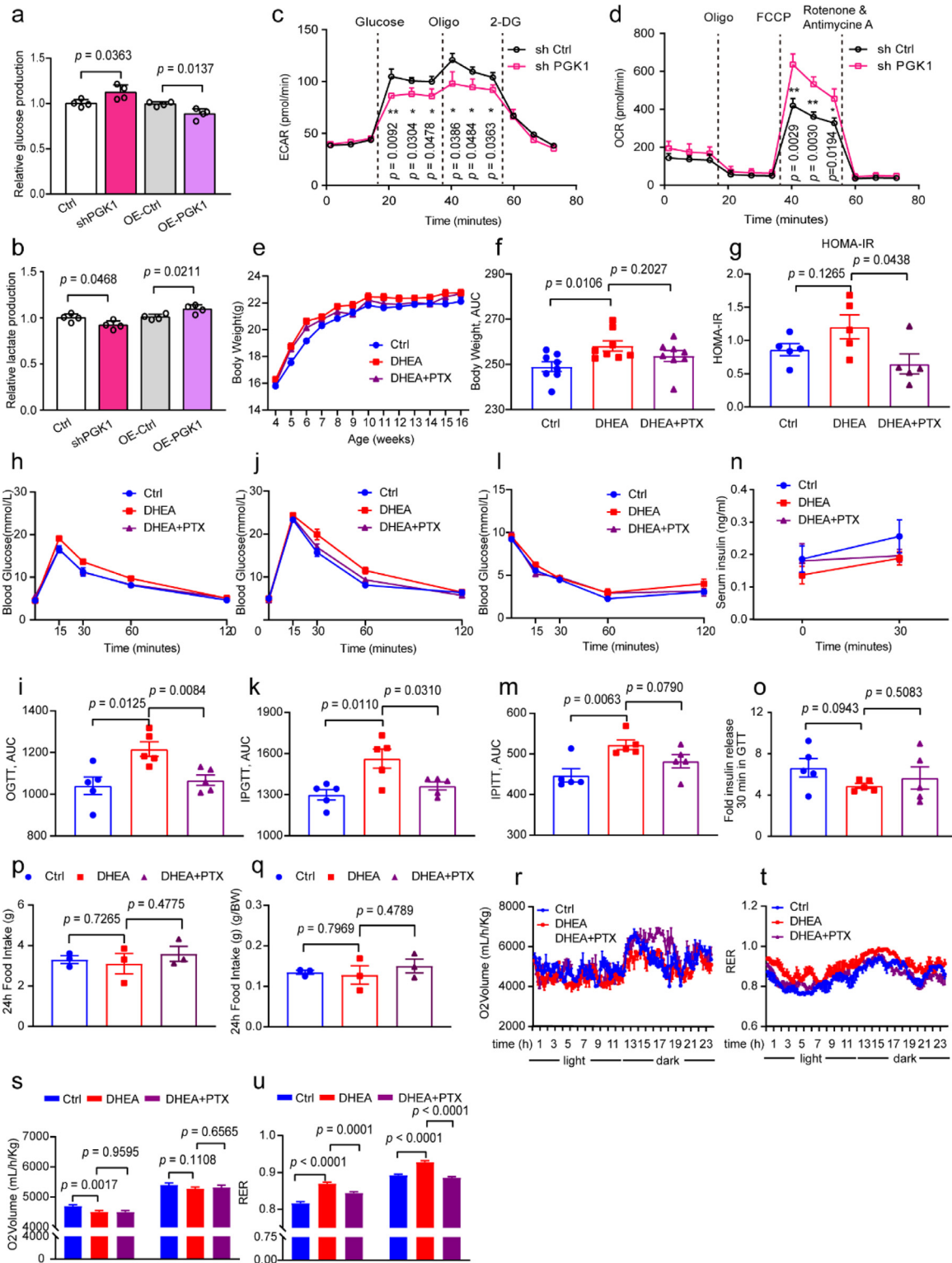


Fig. 3. PGK1 mediates glucose metabolism in cells and aggravates PCOS-like mouse metabolic disorder. (a) Glucose levels in shPGK1 (PGK1 knockdown) and OE-PGK1 (PGK1 over-expression) KGN cells compared with Ctrl (control) KGN cells, $n = 4$. (b) Relative lactate levels in shPGK1 and OE-PGK1 KGN cells compared with Ctrl, $n = 4$. (c-d) Extracellular acidification rates (ECARs) and oxygen consumption rates (OCRs) in shPGK1 and Ctrl KGN cells. Data are expressed as the mean \pm SE. Statistical analysis was performed using an unpaired two-tailed Student's t -test ($*p < 0.05$, $**p < 0.01$). (e) Weight curves for Ctrl (control), PCOS (PCOS-like model mice), and PCOS+PTX (PCOS-like model mice treated with PTX) mice were recorded from 4 weeks to 16 weeks of age, $n = 8$. (f) Area under the curve (AUC) analysis of the three groups. (g) Homeostasis model assessment-insulin resistance (HOMA-IR) was analysed based on fasting blood glucose and insulin levels, $n = 5$. (h-k) Glucose tolerance tests and AUCs were assessed for the three groups, $n = 5$. (i-m) Insulin tolerance test and AUCs for mice in the three groups, $n = 5$. (n-o) Serum insulin levels after 30 min of fasting and the fold changes in serum insulin levels after glucose injection, $n = 5$. (p-q) Cumulative food intake over 24 h, and cumulative food intake normalised to body weight, $n = 3$. (r-s) Consumed O₂ was measured in the three groups during light and dark phases; the histogram represents the mean \pm SE of three mice per group. (t-u) RER was measured during light and dark phases; the histogram represents the mean \pm SE of three mice per group. Three treatment groups of mice: Ctrl (control), PCOS (PCOS-like model mice), and PCOS+PTX (PCOS-like model mice treated with PTX). Statistical analysis was performed by an unpaired two-tailed t -test compared with relevant controls.

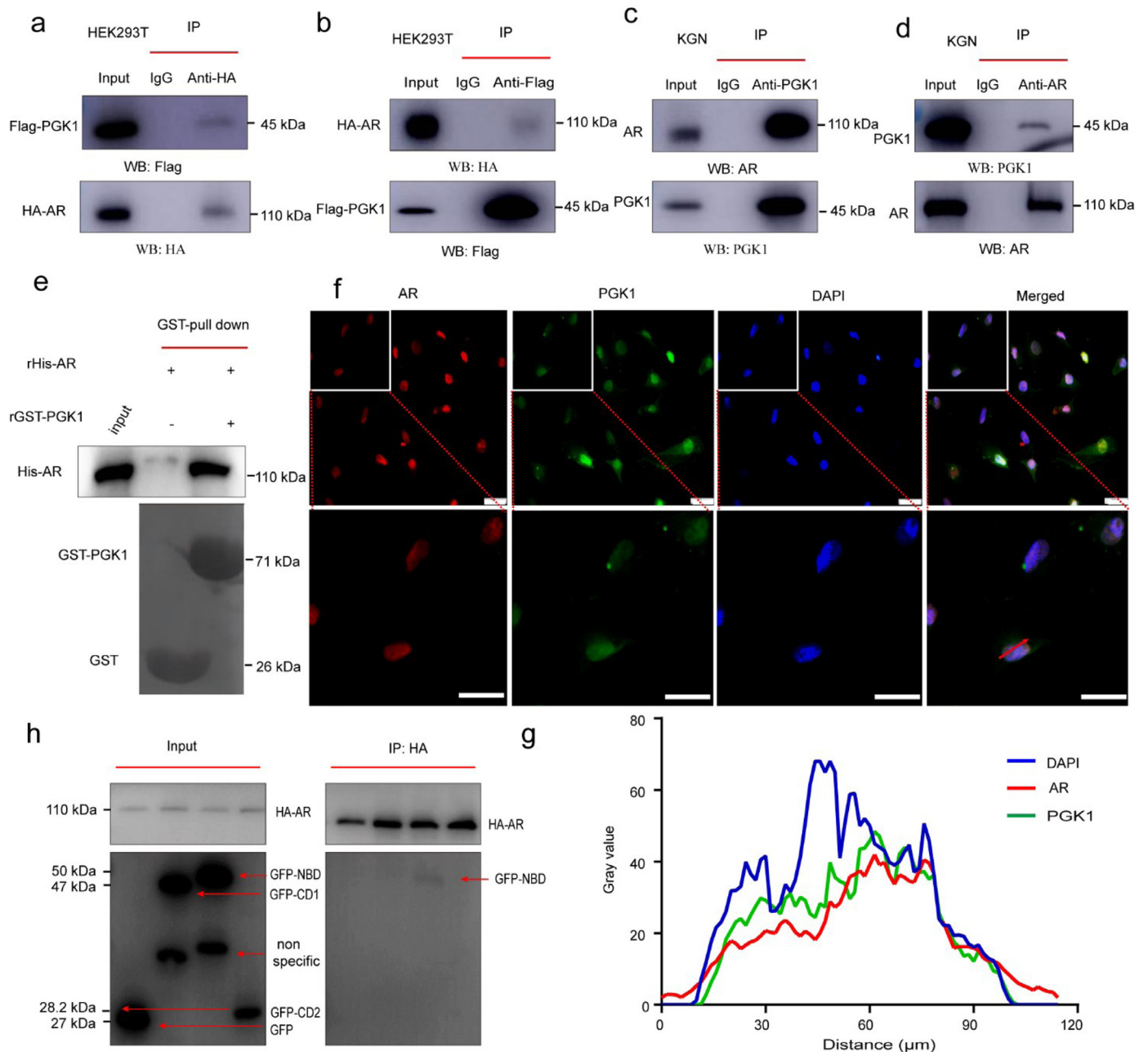


Fig. 4. PGK1 interacts with AR, both in vitro and in vivo. (a–b) HEK293T cells were transfected with HA-AR and Flag-PGK1. The immunoprecipitation interaction assay between HA-AR and Flag-PGK1 was performed by western blotting analysis. The input was used as the positive control and IgG was used as the negative control. (c–d) The endogenous immunoprecipitation interaction assay between PGK1 and AR was performed in KGN cells, and analysed by western blotting. The input was used as the positive control and IgG was used as the negative control. (e) PGK1 binding to AR in vitro, using the GST pull-down assay. The control GST and GST-PGK1 fusion protein were purified with GST-agarose, after being mixed with purified His-AR protein and the interaction was detected by western blotting. (f) Immunofluorescence images of KGN cells illustrate that PGK1 (green) co-localizes with AR (red) in the nucleus. Nuclear DNA was counterstained with DAPI (blue). Scale bars: 200 μm . (g) Line scans of a cell co-stained against PGK1, AR, and DNA, at the position shown by the arrow. (h) An immunoprecipitation assay performed in HEK293T cells showed that AR primarily interacts with the PGK1 NBD domain.

3.6. PGK1 promotes the transcriptional activity of *ar* and ovulation-related gene expression

To further explore the genes regulated by PGK1, a volcano plot and heatmap showing differentially expressed genes were constructed from RNA-seq data, comparing between KGN cells treated with shCtrl+DHT and KGN cells treated with shPGK1+DHT (Figs. 6a and 6b; Supplementary Table 3). From the Venn diagram and heatmap data, we found that 3089 genes regulated by PGK1 were dependent on DHT (Figs. 6c and 6d; Supplementary Table 4). To determine AR target genes, we compared the differentially expressed genes identified between shPGK1+DHT and shCtrl+DHT cells with the AR-

regulated genes reported by Cato et al. [25]. According to the Venn diagram, 190 AR target genes were regulated by PGK1 and dependent on DHT (Figs. 6e and 6f; Supplementary Table 5), indicating that PGK1 regulates AR nuclear translocation and may influence the excessive expression levels of AR-related genes.

To determine which ovulation-related genes were regulated by PGK1, we compared the differentially expressed genes identified from the shPGK1+DHT and shCtrl+DHT comparison with the ovulation-regulated genes expressed in GCs, as reported by Zhang et al. [26]. The Venn diagram and heatmap show that 87 ovulation-related genes were likely regulated by PGK1 (Figs. 6g and 6h; Supplementary Table 6). To further verify the ovulation-related genes

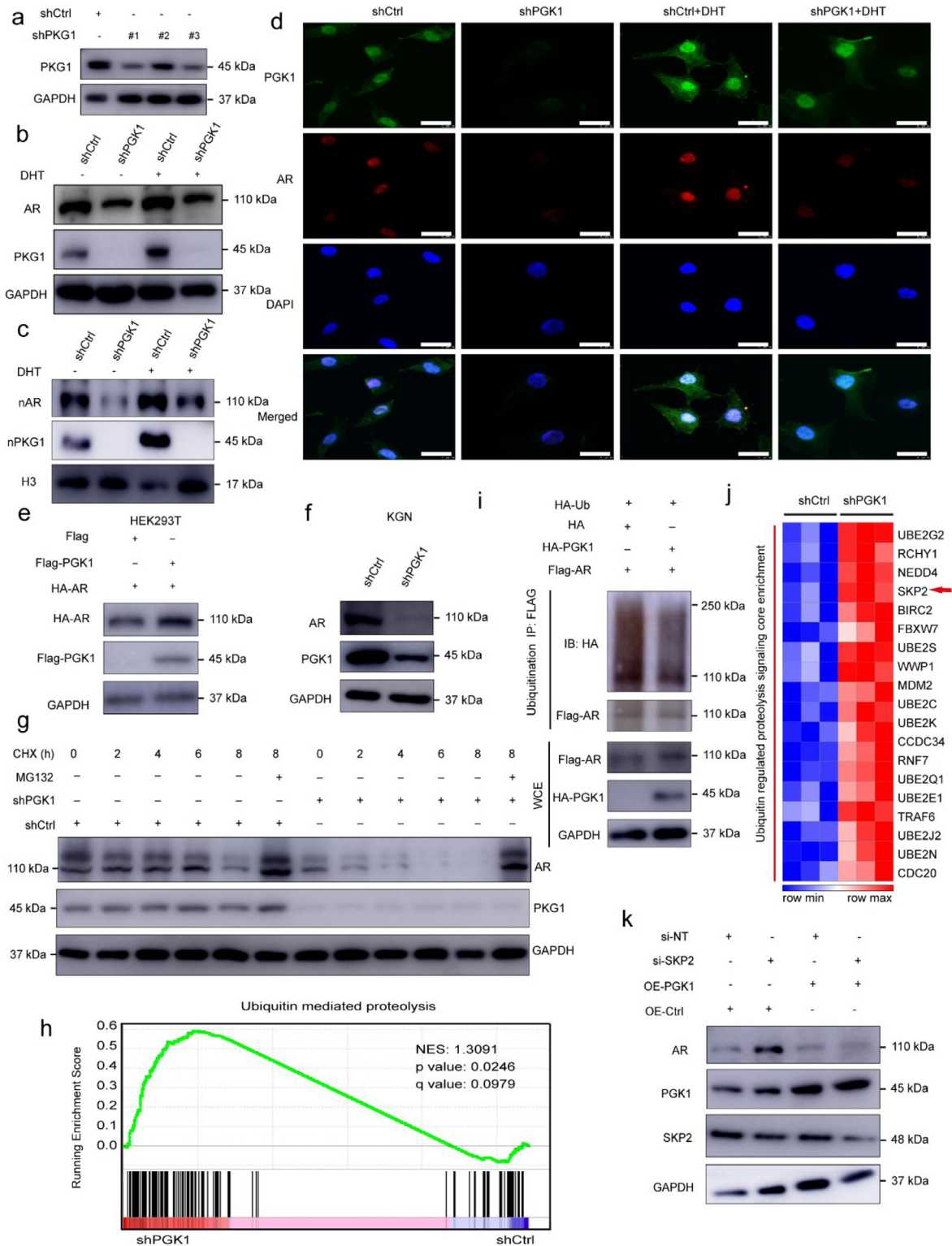


Fig. 5. PGK1 promotes AR translocation into the nucleus and increases AR stability, which depends on the E3 ubiquitin ligase SKP2. (a) Screening and validation of the knockdown shRNA of PGK1 by western blotting. (b) Total PGK1 and AR proteins were detected by western blotting analysis after KGN cells were treated with shPGK1. (c) Nuclear-localized PGK1 and AR proteins were detected by western blotting analysis after KGN cells were treated with shPGK1. (d) The immunofluorescence assay shows that PGK1 promotes AR translocation into the nucleus, in a DHT-dependent manner. KGN cells were fixed with 4% paraformaldehyde and stained with PGK1 and AR antibodies. DAPI was used to stain the nucleus. Scale bars: 200 μ m. (e) Western blotting analysis was used to detect total protein expression levels in HEK293T cells transfected with HA-AR and either Flag-vector or Flag-PGK1. (f) Total PGK1 and AR proteins were detected by western blotting analysis in KGN cells treated with shCtrl or shPGK1. (g) The total AR and PGK1 proteins in KGN cells were analysed by western blotting analysis. The cells were treated with PGK1 shRNA, followed by either cycloheximide or MG132, at the indicated time points. (h) GSEA analysis of the ubiquitin mediated proteolysis pathway in KGN cells treated with shPGK1 compared to Control (shCtrl). (i) AR polyubiquitination was detected by western blotting. HA or HA-PGK1, Flag-AR, and HA-Ub were transfected into HEK293T cells. (j) Primary enrichment genes associated with the ubiquitin-regulated proteolysis pathway were identified in shPGK1 treated KGN cells. The arrow indicates that SKP2 was increased in PGK1 knockdown cells. (k) KGN cells were transfected with PGK1 or si-SKP1, and the total protein levels for AR, PGK1, and SKP2 were analysed by western blotting.

regulated by the PGK1-AR axis, we constructed a Venn diagram between the ovulation-related and AR target genes mediated by PGK1 and found that *MAP2K6*, *MYOF*, *KLF15*, and *LRIG3* were both ovulation-related genes and AR target genes (Fig. 6i). Using qRT-PCR, we verified that these four ovulation-related genes were dependent on DHT and regulated by PGK1 in cells (Fig. 6j), and that PTX could rescue the expression levels in these four genes in PCOS-like mouse ovaries to almost the control level (Fig. 6k). Furthermore, qRT-PCR further confirmed that AR target and ovulation genes were regulated by PGK1 in cells, and that PTX could rescue above the expression levels of these genes in PCOS-like mouse ovaries to the control levels (Supplementary Figure 4). All in all, this indicates that ovulation related genes *MAP2K6*, *MYOF*, *KLF15* and *LRIG3* are regulated by the PGK1-AR axis, and the reason that the PCOS-like phenotype was rescued by PTX to the control level was probably due to improvement of expression of the related target genes regulated by the axis.

3.7. PGK1 inhibits apoptosis and promotes cell proliferation in KGN cells

Next, we used shPGK1 and DHT to treat KGN cells to see the PGK1 effects on cell proliferation and apoptosis. The TUNEL assay showed that PGK1 inhibits apoptosis in cell lines (Figs. 7a and 7b). Western blot analysis further demonstrated that PGK1 regulated the expression of the apoptosis markers caspase 9/cleaved caspase 9, Bcl2 and Bax, resulting in the inhibition of apoptosis (Figs. 7c and 7d). In addition, the effects of PGK1 on cell proliferation were detected by CCK-8 (Fig. 7e), a colony formation assay (Figs. 7f and 7g), and a Bromodeoxyuridine (BrdU) assay (Figs. 7h and 7i). The data indicate that PGK1 promoted cell proliferation and that such proliferation was dependent on DHT. Taken together, these results suggest that PGK1 may suppress apoptosis and enhance GC proliferation, resulting in ovulatory dysfunction.

4. Discussion

Our findings demonstrate that the interaction between PGK1 and AR in GC nuclei may play a sizeable role in the development of ovulation disorders. We provide convincing evidence to support this conclusion. Our data also demonstrate that PGK1 binds directly with AR and that the expression levels of these two proteins were high in human clinical samples of luteinized GCs and ovarian tissues from PCOS-like mice. PGK1 inhibited AR ubiquitination, and PGK1 was dependent on the E3 ligase SKP2 to increase AR stability. In addition, PGK1 promoted AR translocation into the nucleus, and from the deep analysis of RNA-seq and qRT-PCR data, we concluded that AR transcription activity and the expression of critical ovulation-related genes, including *MAP2K6*, *KLF15*, *LRIG3*, and *MYOF*, were regulated by the PGK1-AR axis. High PGK1 expression enhanced glycolysis and metabolic flux, which are regulated by mitogen-activated protein kinase 6 (*MAP2K6*) signaling, resulting in the development of ovulation disorders. However, normal PGK1 levels and AR and ovulation target genes remain in a stable balance, which results in normal metabolism and ovulation (Fig. 8). The PCOS-like mice demonstrated metabolic disorders, including dysfunctional whole-body glucose homeostasis and insulin resistance, which could be partially rescued by PTX treatment. These findings suggest that the PGK1-AR axis may be a promising drug target for PCOS treatment, providing novel insights into the role played by the glycolysis pathway during PCOS-associated metabolic dysfunction.

PCOS is the most common endocrine and metabolic disorder in reproductive-age women. It can lead to hirsutism, anovulatory infertility, and miscarriage, and is characterised by hyperandrogenemia, ovulatory dysfunction, and polycystic ovaries [2, 27–29]. PCOS is also associated with other non-reproductive abnormalities, such as metabolic syndrome, insulin resistance, and dyslipidemia [30–32].

Potential mechanisms associated with PCOS development have been studied [33–35]; however, because of the heterogeneous and comprehensive nature of the endocrine disorders associated with PCOS, the pathogenesis has not yet been fully explained by any reported mechanism. Lack of a dominant follicle is one of most important typical hallmarks in women with PCOS and the relevant outcome is ovulation dysfunction and infertility. Meanwhile, we discovered key glucose metabolism protein kinase PGK1 as a new binding partner with AR in this study. Whether this PGK1-AR axis regulates ovulation dysfunction associated with metabolic disorders is an intriguing issue.

The metabolic reprogramming enzyme PGK1 has become a molecular hotspot, and many reports have focused on the activity of this metabolic enzyme and the effects of PGK1 post-translational modifications (PTMs) during cancer [36,37]. PGK1 converts 1,3-bisphosphoglycerate into 3-phosphoglycerate in the glycolysis pathway, resulting in the production of the first ATP molecule; therefore, PGK1 can control the synthesis of energy and metabolic products [10,38]. Here, we found that *PGK1* mRNA expression levels were higher in PCOS luteinized GCs than in non-PCOS GCs. PGK1 and AR protein expression levels were high in PCOS GCs, suggesting that PCOS may be closely associated with PGK1 and AR protein expression. In our previous study, the treatment of the primary GCs with DHT caused AR translocation into the nucleus, and DHT had a similar promoting effect on AR signaling in prostate cancer [39,40]. Interestingly, in the present study, PGK1 was closely associated with serum testosterone levels, promoted AR translocation into the nucleus, and increased AR stability via physical interactions. The excessive expression of the ovulation-related genes *MAP2K6*, *KLF15*, *LRIG3*, and *MYOF* may be regulated by this critical non-metabolic function of PGK1.

To treat PGK1-associated PCOS, we used PTX as a potential PGK1-targeting drug in a rodent PCOS-like model. Intriguingly, PCOS-like mice presented with metabolic disorders, including glucose homeostasis dysfunction, insulin resistance, and dyslipidemia, which could be partially rescued by PTX treatment (Fig. 3 and Supplementary Figure 5). In addition, PGK1 protein levels were decreased in the cell line treated with PTX, and PGK1 and AR levels were also reduced in the ovaries of PCOS-like mice treated with PTX. This treatment relieved the ovulation disorder and metabolic symptoms observed in the model, and further indicated that the PGK1-AR axis associated metabolism played a vital role in ovulation dysfunction. In the GCs, *c-Fos/AP1* signaling plays a key role in ovulation and a pivotal role in the upregulation of critical ovulatory gene expression; MAPK signaling triggers the response of the ovulation-associated genes *c-Fos* and *c-Jun* [41,42]. Thus, we hypothesised that the PGK1-AR axis regulated metabolic flux and ovulatory dysfunction, primarily via the MAPK signaling family member *MAP2K6*. The medicine rescued PCOS-like mouse phenotype did regulate *c-Fos* and *c-Jun* signaling. Conversely, it demonstrated that phospho-p38 signaling was really regulated by the PGK1-AR axis in the cell line, and the medicine rescued PCOS-like mouse phenotype was probably via this axis in the regulated phospho-p38 signaling pathway in the ovaries (Supplementary Figure 6). Of note, *MAP2K6* is a key upstream regulator of the MAPK signaling molecule p38, which controls cell differentiation and apoptosis, and p38 signaling also heightens glycolysis [43,44]. In this study, PGK1 actually inhibited GC apoptosis by regulating the apoptosis markers PARP, caspase 9/cleaved caspase 9, and Bax, and GC apoptosis could be rescued by PTX treatment, which can cause cell apoptosis by arresting the cell phase [22]. As we know, the GCs play a critical role in the development of the oocytes, as they provide nutrients and growth factors for follicular maturation, and the GCs preferentially metabolize glucose to lactate under anaerobic conditions to support gonadotropin-induced cell differentiation [45]. As we know, excess androgen, insulin resistance, and obesity associations in PCOS may contribute to the development of local and systemic oxidative stress, which may reciprocally worsen

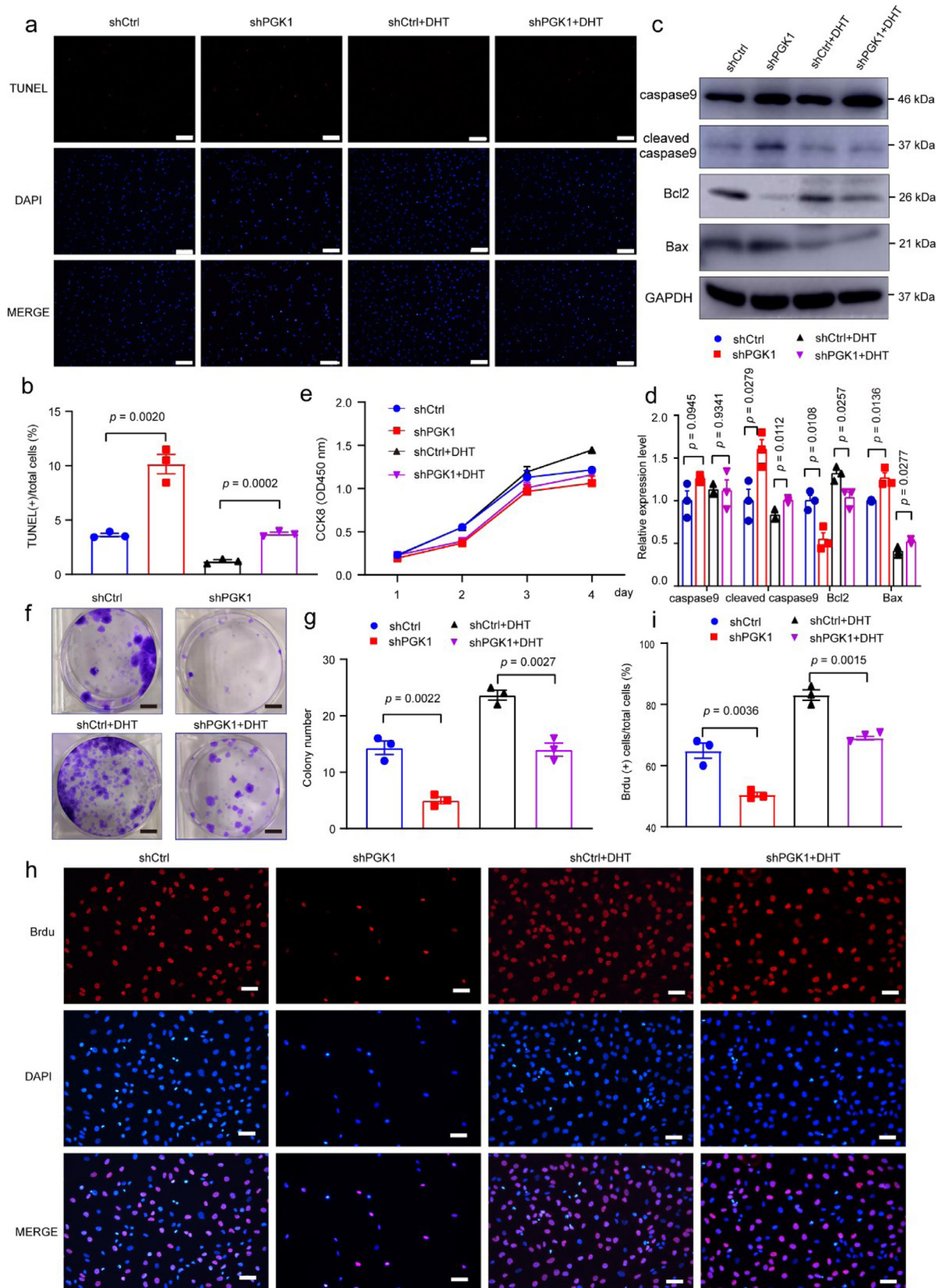


Fig. 7. PGK1 inhibits apoptosis and enhances cell proliferation. (a-b) Representative images of TUNEL assays in indicated KGN cells. Scale bar: 300 μ m. Data are presented as the mean \pm SE, $n = 3$. There were four treatment groups for cells, shCtrl: shRNA control; shPGK1: PGK1 shRNA; Ctrl+DHT: shCtrl treated with DHT for 24 hrs; and shPGK1+DHT: shPGK1 treated with DHT for 24 hrs. (c-d) c-cas9, cas9, Bcl2 and Bax were detected by western blotting analysis following the indicated treatments in KGN cells. Data are presented as the mean \pm SE, $n = 3$. (e) Cell Counting Kit-8 assays were performed following the indicated treatments in KGN cells ($n = 3$). (f-g) Representative images and the quantification of cell colonies in indicated KGN cells. Scale bar: 1 cm. Data are presented as the mean \pm SE, $n = 3$. (h-i) Representative images and the quantification of BrdU (+) in indicated cells. Scale bar: 200 μ m. Data are presented as the mean \pm SE, $n = 3$. Statistical analysis was performed by an unpaired two-tailed t -test compared with relevant controls.

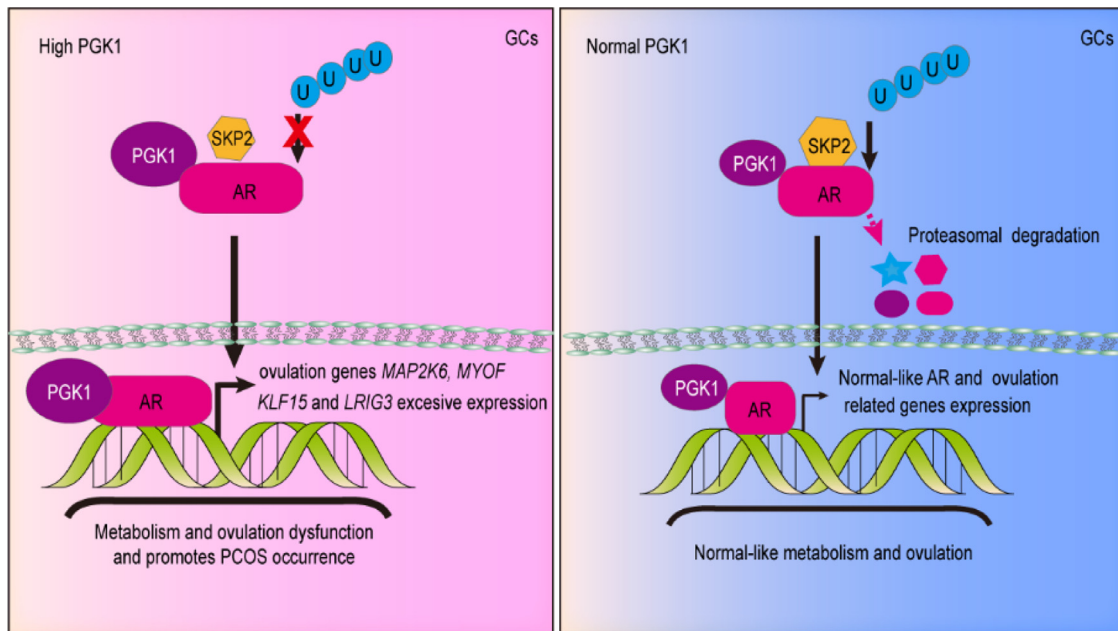


Fig. 8. Proposed model of effect of the PGK1-AR axis during ovulatory dysfunction. High PGK1 in GCs inhibits the AR ubiquitination level, and depends on the E3 ligase SKP2 to increase AR stability. PGK1 promotes AR translocation into the nucleus, and results in excessive AR transcription activity and the expression of critical ovulation-related genes, including *MAP2K6*, *KLF15*, *LRIG3* and *MYOF*, which leads to metabolism and ovulation dysfunction and promotes PCOS occurrence. However, a normal PGK1 level ensures that AR and ovulation related genes remain in a stable balance, and results in normal metabolism and ovulation.

PCOS-associated metabolic abnormalities [30,46]. Our data indicate that PGK1 had a role not just in mediating the follicular microenvironment energy flux via regulating glycolysis in GCs, but also in influencing the function of the mitochondria associated genes' expression and the free radicals in GCs (Supplementary Figure 7), which further demonstrates that energy metabolism and oxidative stress dysfunction aggravated the imbalance of the GC environment. It suggests that the excessive PGK1-AR-MAP2K6 p38 axis likely regulates metabolic flux in GCs and p38 further stimulates glycolysis in GCs, which upsets the GC microenvironment balance and results in dysfunctional ovulation.

Ubiquitination generally promotes protein degradation and represents a classical, regulated PTM, with a critical role in both physiological and pathological processes, such as reproduction, growth and development, signal transduction, and tumorigenesis [47-50]. AR is a nuclear receptor family member with a high-affinity site for chromatin that regulates transcriptional activity, and the ubiquitination ligase system plays a key role in mediating AR activation/reactivation [51-53]. The E3 ligase SKP2 not only plays a vital role in protein degradation via the proteasome but also contributes to cell cycle regulation [54-56]. AR and AR PTMs play important roles in follicular development [6,57]. However, whether the critical glycolysis kinase PGK1 promotes AR stability via PTMs and whether increased AR stability affects the prevalence of ovulation disorders or PCOS remain unclear. Our data indicate that PGK1 was dependent on the E3 ligase SKP2 to promoter AR stability and the PGK1-AR axis-mediated regulation of dysfunctional ovulation via MAP2K6 signaling was likely dependent on SKP2. Thus, we inferred that PGK1-AR together with SKP2 regulated the GC cell cycle, resulting in GC cell cycle arrest, and further caused disordered folliculogenesis. As PGK1 is a protein kinase, we also detected the phosphorylation levels of AR regulated by PGK1, and found that there were no phosphorylation changes (Supplementary Figure 8), indicating that PGK1 regulated AR mainly through protein interactions.

In conclusion, to our knowledge, this is the first report showing the effects of the key GC glycolysis-associated protein kinase PGK1 on disordered folliculogenesis, and that the PGK1-AR axis may be a potential therapeutic target for PCOS.

5. Contributors

H.H., C.Y., J.S., X.L. and G.D. designed the experiments. X.L., C.S., H. G., Z.Z., Z.Y., C.Y. and Y.T. performed the experiments. K.Z. and C.L. analyzed the RNA-seq data. X.L., N.Q. and Y.M. collected the clinical samples and analyzed the characteristics of the clinical patients. Y.Z. and Y.W. performed the animal experiments. X.C. performed partial experiments of supplemental data. C.Y. and H.H. wrote the paper with the help of the authors. We declare that all authors read and approved the final version of the manuscript.

Declaration of Competing Interest

The authors declare that they have no competing interests.

Supplementary materials

Supplementary material associated with this article can be found, in the online version, at [doi:10.1016/j.ebiom.2020.103058](https://doi.org/10.1016/j.ebiom.2020.103058).

References

- [1] Norman RJ, Dewailly D, Legro RS, Hickey TE. Polycystic ovary syndrome. *Lancet* 2007;370(9588):685-97.
- [2] Escobar-Morreale HF. Polycystic ovary syndrome: definition, aetiology, diagnosis and treatment. *Nat Rev Endocrinol* 2018;14(5):270-84.
- [3] Tanos T, Marinissen MJ, Leskow FC, et al. Phosphorylation of c-Fos by members of the p38 MAPK family. Role in the AP-1 response to UV light. *J. Biol. Chem.* 2005;280(19):18842-52.
- [4] Sharma SC, Richards JS. Regulation of AP1 (Jun/Fos) factor expression and activation in ovarian granulosa cells. Relation of JunD and Fra2 to terminal differentiation. *J. Biol. Chem.* 2000;275(43):33718-28.
- [5] Angel P, Karin M. The role of Jun, Fos and the AP-1 complex in cell-proliferation and transformation. *Biochim. Biophys. Acta* 1991;1072(2-3):129-57.
- [6] Sen A, Hammes SR. Granulosa cell-specific androgen receptors are critical regulators of ovarian development and function. *Molecular endocrinology* (Baltimore, Md) 2010;24(7):1393-403.
- [7] Ni L, Llewellyn R, Kesler CT, et al. Androgen induces a switch from cytoplasmic retention to nuclear import of the androgen receptor. *Mol. Cell. Biol.* 2013;33(24):4766-78.
- [8] Yu CJ, Liu X, Zhou ZY, et al. The casein kinase 2alpha promotes the occurrence polycystic ovary syndrome. *Biochem Biophys Res Commun* 2020;525:121-8.

- [9] Lu Z, Hunter T. Metabolic Kinases Moonlighting as Protein Kinases. *Trends Biochem Sci* 2018;43(4):301–10.
- [10] Bernstein BE, Hol WG. Crystal structures of substrates and products bound to the phosphoglycerate kinase active site reveal the catalytic mechanism. *Biochemistry* 1998;37(13):4429–36.
- [11] Shichijo S, Azuma K, Komatsu N, et al. Two proliferation-related proteins, TYMS and PGK1, could be new cytotoxic T lymphocyte-directed tumor-associated antigens of HLA-A2+ colon cancer. *Clin Cancer Res* 2004;10(17):5828–36.
- [12] Fu D, He C, Wei J, et al. PGK1 is a Potential Survival Biomarker and Invasion Promoter by Regulating the HIF-1 α -Mediated Epithelial-Mesenchymal Transition Process in Breast Cancer. *Cell Physiol Biochem* 2018;51(5):2434–44.
- [13] Qian X, Li X, Lu Z. Protein kinase activity of the glycolytic enzyme PGK1 regulates autophagy to promote tumorigenesis. *Autophagy* 2017;13(7):1246–7.
- [14] Hu H, Zhu W, Qin J, et al. Acetylation of PGK1 promotes liver cancer cell proliferation and tumorigenesis. *Hepatology (Baltimore, Md)* 2017;65(2):515–28.
- [15] Zhang Y, Yu G, Chu H, et al. Macrophage-Associated PGK1 Phosphorylation Promotes Aerobic Glycolysis and Tumorigenesis. *Mol Cell* 2018;71(2):201–15.e7.
- [16] O'Reilly MW, Kempegowda P, Walsh M, et al. AKR1C3-Mediated Adipose Androgen Generation Drives Lipotoxicity in Women With Polycystic Ovary Syndrome. *J Clin Endocrinol Metab* 2017;102(9):3327–39.
- [17] Risal S, Pei Y, Lu H, et al. Prenatal androgen exposure and transgenerational susceptibility to polycystic ovary syndrome. *Nat Med* 2019;25(12):1894–904.
- [18] Yu C, Dou K, Wang S, et al. Elicitor hydrophobin Hyd1 interacts with Ubiquitin1-like to induce maize systemic resistance. *J Integr Plant Biol* 2020;62(4):509–26.
- [19] Qi X, Yun C, Sun L, et al. Gut microbiota-bile acid-interleukin-22 axis orchestrates polycystic ovary syndrome. *Nat Med* 2019;25(8):1225–33.
- [20] Magaki S, Hojat SA, Wei B, So A, Yong WH. An Introduction to the Performance of Immunohistochemistry. *Methods Mol Biol* 2019;1897:289–98.
- [21] Chakraborty P, Vaena SG, Thyagarajan K, et al. Pro-Survival Lipid Sphingosine-1-Phosphate Metabolically Programs T Cells to Limit Anti-tumor Activity. *Cell Rep* 2019;28(7):1879–93.e7.
- [22] Wan X, Beaudoin JJ, Vinod N, et al. Co-delivery of paclitaxel and cisplatin in poly(2-oxazoline) polymeric micelles: implications for drug loading, release, pharmacokinetics and outcome of ovarian and breast cancer treatments. *Biomaterials* 2019;192:1–14.
- [23] Ho MY, Tang SJ, Ng WV, et al. Nucleotide-binding domain of phosphoglycerate kinase 1 reduces tumor growth by suppressing COX-2 expression. *Cancer Sci* 2010;101(11):2411–6.
- [24] Zheng N, Shabek N. Ubiquitin Ligases: structure, Function, and Regulation. *Annu Rev Biochem* 2017;86:129–57.
- [25] Cato L, Neeb A, Sharp A, et al. Development of Bag-1 L as a therapeutic target in androgen receptor-dependent prostate cancer. *Elife* 2017;6:e27159.
- [26] Zhang Y, Yan Z, Qin Q, et al. Transcriptome Landscape of Human Folliculogenesis Reveals Oocyte and Granulosa Cell Interactions. *Mol Cell* 2018;72(6):1021–34.e4.
- [27] Homburg R. What is polycystic ovarian syndrome? A proposal for a consensus on the definition and diagnosis of polycystic ovarian syndrome. *Hum Reprod* 2002;17(10):2495–9.
- [28] Somani N, Turvy D. Hirsutism: an evidence-based treatment update. *Am J Clin Dermatol* 2014;15(3):247–66.
- [29] Azziz R, Carmina E, Chen Z, et al. Polycystic ovary syndrome. *Nat Rev Dis Primers* 2016;2:16057.
- [30] Skiba MA, Islam RM, Bell RJ, Davis SR. Understanding variation in prevalence estimates of polycystic ovary syndrome: a systematic review and meta-analysis. *Hum Reprod Update* 2018;24(6):694–709.
- [31] Kakoly NS, Khomami MB, Joham AE, et al. Ethnicity, obesity and the prevalence of impaired glucose tolerance and type 2 diabetes in PCOS: a systematic review and meta-regression. *Hum Reprod Update* 2018;24(4):455–67.
- [32] Luque-Ramirez M, Nattero-Chavez L, Ortiz Flores AE, Escobar-Morreale HF. Combined oral contraceptives and/or antiandrogens versus insulin sensitizers for polycystic ovary syndrome: a systematic review and meta-analysis. *Hum Reprod Update* 2018;24(2):225–41.
- [33] Rosenfield RL, Ehrmann DA. The Pathogenesis of Polycystic Ovary Syndrome (PCOS): the Hypothesis of PCOS as Functional Ovarian Hyperandrogenism Revisited. *Endocr Rev* 2016;37(5):467–520.
- [34] Murri M, Luque-Ramirez M, Insenser M, Ojeda-Ojeda M, Escobar-Morreale HF. Circulating markers of oxidative stress and polycystic ovary syndrome (PCOS): a systematic review and meta-analysis. *Hum Reprod Update* 2013;19(3):268–88.
- [35] Diamanti-Kandarakis E, Dunaif A. Insulin resistance and the polycystic ovary syndrome revisited: an update on mechanisms and implications. *Endocr Rev* 2012;33(6):981–1030.
- [36] He Y, Luo Y, Zhang D, et al. PGK1-mediated cancer progression and drug resistance. *Am J Cancer Res* 2019;9(11):2280–302.
- [37] Nie H, Ju H, Fan J, et al. O-GlcNAcylation of PGK1 coordinates glycolysis and TCA cycle to promote tumor growth. *Nat Commun* 2020;11(1):36.
- [38] Qian X, Li X, Shi Z, et al. PTEN Suppresses Glycolysis by Dephosphorylating and Inhibiting Autophosphorylated PGK1. *Mol Cell* 2019;76(3):516–27.e7.
- [39] Dai J, Shen R, Sumitomo M, et al. Synergistic activation of the androgen receptor by bombesin and low-dose androgen. *Clin Cancer Res* 2002;8(7):2399–405.
- [40] Wang F, Pan J, Liu Y, et al. Alternative splicing of the androgen receptor in polycystic ovary syndrome. *Proc Natl Acad Sci U S A* 2015;112(15):4743–8.
- [41] Talbott H, Delaney A, Zhang P, et al. Effects of IL8 and immune cells on the regulation of luteal progesterone secretion. *Reproduction* 2014;148(1):21–31.
- [42] Choi Y, Rosewell KL, Brannstrom M, Akin JW, Curry Jr. TE, Jo M. FOS, a Critical Downstream Mediator of PGR and EGF Signaling Necessary for Ovarian Prostaglandins in the Human Ovary. *J Clin Endocrinol Metab* 2018;103(11):4241–52.
- [43] Liu J, Wen D, Fang X, Wang X, Liu T, Zhu J. p38MAPK Signaling Enhances Glycolysis Through the Up-Regulation of the Glucose Transporter GLUT-4 in Gastric Cancer Cells. *Cell Physiol Biochem* 2015;36(1):155–65.
- [44] Gills JJ, Castillo SS, Zhang C, et al. Phosphatidylinositol ether lipid analogues that inhibit AKT also independently activate the stress kinase, p38 α , through MKK3/6-independent and -dependent mechanisms. *J Biol Chem* 2007;282(37):27020–9.
- [45] Campbell BK, Onions V, Kendall NR, Guo L, Scaramuzzi RJ. The effect of monosaccharide sugars and pyruvate on the differentiation and metabolism of sheep granulosa cells in vitro. *Reproduction* 2010;140(4):541–50.
- [46] Victor VM, Rocha M, Banuls C, et al. Induction of oxidative stress and human leukocyte/endothelial cell interactions in polycystic ovary syndrome patients with insulin resistance. *J Clin Endocrinol Metab* 2011;96(10):3115–22.
- [47] Cheng X, Hao Y, Shu W, et al. Cell cycle-dependent degradation of the methyltransferase SETD3 attenuates cell proliferation and liver tumorigenesis. *J Biol Chem* 2017;292(22):9022–33.
- [48] Bushweller JH. Targeting transcription factors in cancer - from undruggable to reality. *Nat Rev Cancer* 2019;19(11):611–24.
- [49] Crane A, Rape M. Dynamic regulation of ubiquitin-dependent cell cycle control. *Curr Opin Cell Biol* 2013;25(6):704–10.
- [50] Zhang X, Zhang H, Xu C, et al. Ubiquitination of RIPK1 suppresses programmed cell death by regulating RIPK1 kinase activation during embryogenesis. *Nat Commun* 2019;10(1):4158.
- [51] Mangelsdorf DJ, Thummel C, Beato M, et al. The nuclear receptor superfamily: the second decade. *Cell* 1995;83(6):835–9.
- [52] Augello MA, Liu D, Deonarine LD, et al. CHD1 Loss Alters AR Binding at Lineage-Specific Enhancers and Modulates Distinct Transcriptional Programs to Drive Prostate Tumorigenesis. *Cancer Cell* 2019;35(5):817–9.
- [53] De Laere B, Rajan P, Gronberg H, Dirix L, Lindberg J. Androgen Receptor Burden and Poor Response to Abiraterone or Enzalutamide in TP53 Wild-Type Metastatic Castration-Resistant Prostate Cancer. *JAMA Oncol* 2019;5(7):1060–2.
- [54] Cai Z, Moten A, Peng D, et al. The Skp2 Pathway: a Critical Target for Cancer Therapy. *Semin Cancer Biol* 2020.
- [55] Gassen NC, Niemeyer D, Muth D, et al. SKP2 attenuates autophagy through Beclin1-ubiquitination and its inhibition reduces MERS-Coronavirus infection. *Nat Commun* 2019;10(1):5770.
- [56] Jang W, Kim T, Koo JS, Kim SK, Lim DS. Mechanical cue-induced YAP instructs Skp2-dependent cell cycle exit and oncogenic signaling. *EMBO J* 2017;36(17):2510–28.
- [57] Lim JJ, Han CY, Lee DR, Tsang BK. Ring Finger Protein 6 Mediates Androgen-Induced Granulosa Cell Proliferation and Follicle Growth via Modulation of Androgen Receptor Signaling. *Endocrinology* 2017;158(4):993–1004.